Biological in situ characterization of polymeric microbubble contrast agents

Wan, Sha; Egri, Gabriella; Oddo, Letizia; Cerroni, Barbara; Dähne, Lars; Paradossi, Gaio; Salvati, Anna; Lynch, Iseult; Dawson, Kenneth A.; Monopoli, Marco P.

DOI:
10.1016/j.biocel.2016.03.004

Document Version
Peer reviewed version

Citation for published version (Harvard):
Wan, S, Egri, G, Oddo, L, Cerroni, B, Dähne, L, Paradossi, G, Salvati, A, Lynch, I, Dawson, KA & Monopoli, MP 2016, 'Biological in situ characterization of polymeric microbubble contrast agents', *The International Journal of Biochemistry & Cell Biology*. https://doi.org/10.1016/j.biocel.2016.03.004

Title: Biological *in situ* characterization of polymeric microbubble contrast agents

Author: Sha Wan Gabriella Egri Letizia Oddo Barbara Cerroni Lars Dähne Gaio Paradossi Anna Salvati Iseult Lynch Kenneth A. Dawson Marco P. Monopoli

PII: S1357-2725(16)30058-9
DOI: http://dx.doi.org/doi:10.1016/j.biocel.2016.03.004
Reference: BC 4813

To appear in: *The International Journal of Biochemistry & Cell Biology*

Received date: 7-3-2016
Accepted date: 15-3-2016

Please cite this article as: Wan, Sha., Egri, Gabriella., Oddo, Letizia., Cerroni, Barbara., Dähne, Lars., Paradossi, Gaio., Salvati, Anna., Lynch, Iseult., Dawson, Kenneth A., & Monopoli, Marco P., Biological in situ characterization of polymeric microbubble contrast agents.*International Journal of Biochemistry and Cell Biology* http://dx.doi.org/10.1016/j.biocel.2016.03.004

Biological *in situ* characterization of polymeric microbubble contrast agents

Sha Wan[1], Gabriella Egri[2], Letizia Oddo[3], Barbara Cerroni[3], Lars Dähne[2], Gaio Paradossi[3], Anna Salvati[1,4], Iseult Lynch[5], Kenneth A. Dawson[1*] and Marco P. Monopoli[1,6 *]

1 - Centre for BioNano Interactions, School of Chemistry & Chemical Biology, University College Dublin, Belfield, Dublin 4, Ireland
2 - Surflay Nanotec GmbH, Schwarzschildstr, 8, 12489 Berlin, Germany
3 - Dipartimento di Scienze e Tecnologie Chimiche, Università di Roma Tor Vergata. Via della Ricerca Scientifica 00133 Rome, Italy
4 - Groningen Research Institute of Pharmacy, Division Pharmacokinetics, Toxicology and Targeting, University of Groningen, A. Deusinglaan 1, 9713 AV Groningen, The Netherlands
5- School of Geography, Earth and Environmental Sciences, University of Birmingham, Edgbaston, Birmingham B15 2TT, United Kingdom
6- Department of Pharmacy and Medical Chemistry, Royal College of Surgeons in Ireland, 123 St.Stephen Green, Dublin 2, Ireland

** To whom correspondence should be addressed:*
Marco P. Monopoli (marcomonopoli@rcsi.ie)
Kenneth A. Dawson (kenneth.a.dawson@cbni.ucd.ie)
Centre for BioNano Interactions, School of Chemistry and Chemical Biology, University College Dublin, Belfield, Dublin 4, Ireland
Phone: +353 1 716 2459

Graphical abstract

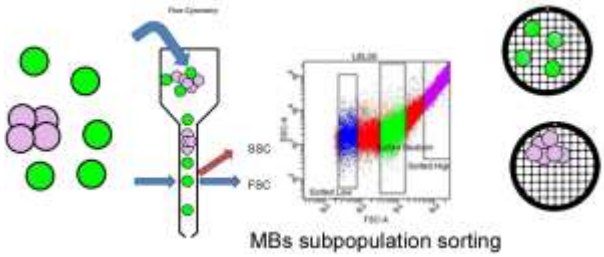

Abstract

Polymeric microbubbles (MBs) are gas filled particles composed of a thin stabilized polymer shell that have been recently developed as valid contrast agents for the combined use of ultrasonography (US), magnetic resonance imaging (MRI) and single photon emission computer tomography (SPECT) imaging. Due to their buoyancy, the commonly available approaches to study their behaviour in complex media are not easily applicable and their use in modern medicine requires to be fully elucidated. Here we have used for the first time flow cytometry as a new high throughput approach that allows to characterize the MB dispersions, prior and after exposure in different biological media and we have additionally developed a method that allows to characterise the strongly bound proteins adsorbed on the MBs, to fully predict their biological behaviour in biological milieu.

Keywords: microbubbles, protein corona, flow cytometry, opsonin proteins, disopsonin proteins, bionano interactions

1. Introduction

Recent advances in nano and micro-material research have made possible many applications in modern nanomedicine where various particle types have been developed with the potential use as drug carriers for therapeutic purposes (Ferrari, 2005, Peyratout and Dahne, 2004) and as diagnostic imaging tools (Colvin, 2003, Gao et al. , 2008). It is now well-established that nanomaterials, as also observed for larger biomaterials upon exposure to biological fluids, such as human plasma, are immediately coated by biomolecules that form a biomolecular layer which represent the key to their biological impacts, hereafter called the "protein corona" (Aggarwal et al. , 2009, Maiolo et al. , 2015, Milani et al. , 2012, Monopoli et al. , 2011, Nel et al. , 2009, Rocker et al. , 2009, Tenzer et al. , 2013, Wan et al. , 2015, Yan et al. , 2013). This biomolecular corona is typically composed of an outer weakly interacting layer of proteins (the dynamic corona) (Milani, Baldelli Bombelli, 2012), which is rapidly exchanging with free proteins in the biological milieu, and an inner hard corona of proteins strongly bound to the nanomaterial surface that are slowly exchanging and reside on the surface for longer residence times. Previous studies on several different nanomaterials have shown that from the roughly 3700 proteins present in human plasma, whose abundance varies over several orders of magnitude, only a few tens of proteins with high affinity (for a particular material) are associated with any specific nanomaterial surface with sufficient residence time to provide a biological identity for that nanomaterial (Bigdeli et al. , 2016, Casals et al. , 2010, Cedervall et al. , 2007, Hadjidemetriou et al. , 2015b, Monopoli et al. , 2012, Tenzer, Docter, 2013, Walkey and Chan, 2012, Wan, Kelly, 2015). Thus, the biological machinery is not likely to "see" the pristine surface of such materials (Ge et al. , 2011, Lesniak et al. , 2012, Walczyk et al. , 2010).

The properties of nanomaterials such as their shape, charge, surface chemistry, functional groups and material impact the protein corona composition which may lead to different biological consequences (Sund et al. , 2011, Walkey and Chan, 2012). For example, binding of opsonin proteins (e.g., fibrinogen, complement proteins and immunoglobulins) to particles can lead to recognition by macrophages, (Konduru et al. , 2009) promoting cellular uptake (Lunov et al. , 2011) and inflammation,(Boraschi et al. , 2012, Ishida et al. , 2001) while, binding of disosponin proteins (e.g., serum albumin, transferrin and lipoproteins) is likely to favour prolonged circulation time in the blood stream and may confer improved

biocompatibility of nanomaterials (Camner et al. , 2002, Hadjidemetriou et al. , 2015a, Mahmoudi et al. , 2011, Palchetti et al. , 2016).

Recent studies have shown that other biomolecules form the corona and their component has a strong impact on the biological response. For example Wan and co-authors have recently highlighted the importance of the carbohydrates at the bionano interface (Wan, Kelly, 2015), and increasing studies, using lung lining fluids, have shown how the lipids and the surfactant proteins can modulate the protein corona composition. (Konduru, Tyurina, 2009, Kumar et al. , 2016, Raesch et al. , 2015).

Due to the buoyancy of the MBs, the use of standard physico-chemical characterisation methods and approaches for the MB corona complexes isolation are not easily applicable. We describe here an alternative method which allows the characterization of MB protein coronas in a high throughput manner by means of flow cytometry, a tool used until now mainly in cell biology. By means of this technique we illustrate that flow cytometry is capable of providing information about the MB concentration, on the dispersion properties in complex media and it is also a useful method to isolate MB strongly bound protein corona complexes.

2. Materials and methods

2.1 Microbubbles

The PVA MBs were made of a shell of crosslinked poly(vinyl alcohol), while the Type B MBs were synthesized by embedding iron oxide magnetic nanoparticles into the poly(vinyl alcohol) shell. Various types of layer-by-layer MBs (LBL) were also provided for our studies. These LBL MBs were all multilayer MBs which were made using the same aminoguanidine shell (e.g., LBL02, shell only), but with different specific materials introduced into the aminoguanidine shell (e.g., LBL 03-11). All the above MBs were in the size range 2~4.5 μm and collectively possessed a similar surface curvature. Various coatings on the MB shells were designed to improve their surface functionality, and improve their use as contrast agents. Table 1 provides a summary descriptions of the MBs used in the study in terms of their shell composition and outer surface layer charge.

2.2 Physico-chemical characterization of MBs by flow cytometry

The stock solution of MBs was mixed for 5-10 seconds using a vortex mixer until the MBs were homogeneously dispersed (as determined by visual inspection). 10^6 MBs were diluted in 1ml in relevant media (such as PBS or the biological fluid of choice, such as 6% human plasma, 10% bovine serum, full human plasma and full human blood) and this dose corresponds to a typical dose used for *in vivo* imaging (Brismar et al. , 2012). Following incubation the sample was analysed by flow cytometer using an Accuri C6 system (BD Biosciences). MBs sub-populations were isolated in a FACSAria™ III cell sorter (also from BD). Non-fluorescent MBs were detected by their forward and side scattering. The fluid flow in the flow cytometer was fixed at a speed of 14 µl per minute in all cases.

2.3 Biological fluid

Human plasma was obtained from the Irish Blood Transfusion Service (IBTS), St. James Hospital following their internal procedure. Human blood was obtained from three male and three female healthy donors. After collection the plasma was pooled and stored at -80 °C in 2ml aliquots. Human plasma was tested for total protein content using the bicinchoninic acid assay (BCA assay, Pierce) and for protein dispersion by size exclusion chromatography (data not shown). Foetal bovine serum (FBS) serum was obtained from Gibco (Biosciences, Ireland).

On the day of each experiment, biological fluid was allowed to thaw at room temperature until the solution looked clear, then centrifuged for 3minutes at 16,000 rcf. The plasma was diluted to required concentration in 1mM EDTA phosphate buffered saline (PBS).

2.4 Protein corona isolation from human plasma

For each MB type, MBs were incubated with the biological fluid of choice (6% plasma, 10% serum or ~100% undiluted plasma) for 1 hour at 37ºC under agitation. They were subsequently allowed to float to the surface of the solution for 120 minutes without agitation and the medium below the MBs was carefully removed with a needle-assembled syringe. MB-protein corona complexes were then washed 5 times with 1 ml of PBS (allowing the MBs to float to the surface each time for 30 minutes) to remove loosely bound proteins (the so-called soft corona) in order to isolate only the strongly bound proteins (the so-called hard corona). Prior to running on an SDS-PAGE gel, MB-protein corona complexes were counted using a counting chamber (haemocytometer) in phase contrast microscopy and the number of

MBs were calculated such that identical numbers of each MB type / replicate were applied for the gel loading.

2.5 Sodium dodecyl sulphate polyacrylamide electrophoresis (SDS-PAGE)

To characterize the protein corona formed on the MBs, the isolated MB-protein samples were run in SDS-PAGE gel electrophoresis. Prior to the electrophoresis, the proteins bound to the MBs were denatured and linearized in the presence of surfactant (sodium dodecyl sulphate SDS) and reducing agents (DTT) by boiling the solutions at 95^{o}C for 5 min. The sample then was loaded into a 10 %polyacrylamide gel and the proteins were separated under electric field in the gel matrix according to the protein molecular weight. To detect the protein bands, the gel was stained using silver staining for protein band detection and using coomassie blue staining for mass spectrometry analysis. The separated proteins were then compared with the standard protein ladder to analyze the protein distribution.

2.6 Mass spectrometry

To determine the protein corona composition, the gel lanes containing the protein corona associated with specific MBs were cut out from the gel following SDS-PAGE gel electrophoresis as described above and following by gel based mass spectrometry analysis. The digested protein bands were then re-suspended in 0.1%formic acid. Electrospray liquid chromatography mass spectrometry (LC MS/MS) equipped with an HPLC (Surveyor, ThermoFinnigan, CA) interfaced with an LTQ Orbitrap (ThermoFinnigan, CA) was used to analyze the peptide mixtures following typsin digestion. Spectra were searched with BioworksBrowser 3.3.1 SP1 (ThermoFisher Scientific) using Sequest Uniprot/Swiss-Prot database (www.expasy.org). When the same protein identity was detected in multiple bands from the same samples, their SpCs were summed to get the total protein amount. The spectral count of each protein was then converted into a Normalized Spectral Count (NSpC), expressed as the spectral count in relation to its molecular weight and relative protein amount in percentage, using the following equation(Zybailov et al. , 2006):

$$\mathrm{NpSpC}_k = \left(\frac{(\mathrm{SpC}/M_w)_k}{\sum_{i=1}^{n} (\mathrm{SpC}/M_w)_i} \right) \times 100$$

where $NpSpC_k$ is the percentage of the normalised spectral count for protein *k*, SpC is the spectral count, and M_w is the molecular weight in KDa for protein *k*.

3. Results and Discussion

3.1 Characterization of MBs dispersions by flow cytometry

In this study we have tested two distinct types of MBs, those with a polymer shell of poly(vinyl alcohol) (PVA) and MBs prepared via a layer by layer (LBL) approach (Brismar, Grishenkov, 2012, Cavalieri et al. , 2005, He et al. , 2012, Peyratout and Dahne, 2004). While for the first set of particles, the PVA polymer stabilized the MBs against aggregation (similar to PEG modification), (Cerroni et al. , 2011, de Gennes, 1987) LBL MBs have been modified by layer by layer deposition of polymers on the MBs core. LBL MBs exhibit either a positively or negatively charged surface depending on the peripheral exposed layer and they are electrostatically stabilized due to the repulsion between charged particles. In this study we have tested 10 types of MBs (Table 1), here we discuss the results mainly from 6 examples of MBs: PVA, PVA shelled MBs decorated with iron oxide nanoparticles (Type B), and four types of LBL coated MBs (specifically LBL02, LBL03, LBL04 and LBL08).

MB concentration and size distribution are traditionally determined by confocal laser scanning microscopy, due to their "large" size, which is well above the limits of optical resolution, however this process is laborious and time consuming, as well as low-throughput, making it far from optimal for routine characterization and can potentially lead to statistically unreliable results. Flow cytometry is a routine method for the counting of single objects forced through a flow cell where they are excited by a laser. Forward scattering (FSC) and side scattering (SSC) are measured by detectors that are placed in line and perpendicular to the light source, respectively. While FSC values are directly correlated to the size of a scattering object, the SSC reflects the object complexity, structure and density. Here we have applied flow cytometry to the characterisation of MBs for the first time, allowing larger numbers of MBs to be analysed with greater accuracy and with significantly higher throughput.

By plotting the forward scattering values against the number of scattering objects (Figures 1-4 panel a), it is clear that the MB population consists of sub-populations of particles with low, medium and high FSC intensity, suggesting the presence of both single MBs along with agglomerates. Plotting the SSC against the FSC, it is possible to see that the SSC of these sub-populations is similar (Figures 1-4b). Phase contrast microscopy of the various MB dispersions post-synthesis is shown in Figures 1-4c and confirms the co-existence of clusters

of MBs along with single MBs (Figures 1c and 4c). This is particularly enhanced for LBL08 where large aggregates and MB clusters are detected along with single MBs (Figure 3c), while Type B, LBL03 and PVA samples contain mainly single MBs with only limited small clusters (Figures 1c, 2c and 4c).

Taking advantage of the large size of the MBs which allows detection by flow cytometry, we have also used the same method to sort MB sub-populations with "high" and "medium" forward scattering values have been sorted and separated into different fractions by means of fluorescence-assisted cell sorting (FACS), allowing further characterisation, purification and imaging by phase contrast light microscopy. Phase contrast analysis of the sorted fractions has revealed that the "medium" population contained single (dispersed) MBs (Figures 1-4 e-f) of size ca.~3 µm, while the population with high forward scattering values (ca.~10^5, called "high") contained clusters of MBs or large aggregates as expected (Figures 1-4 d).

A similar strong correlation between the measured FSC values (Figures 1-4 a-b) and the MBs dispersion stated observed by imaging (Figures 1-4 c-f) was confirmed for all the MB samples studied. For example, flow cytometry FSC values have indicated that LBL08 MBs contained a population of large MB aggregates (Figure 3a-b), and this was also confirmed by image analysis (Figure 3c). This can be explained by the outmost chitosan layer having a pK_a value of 6.3 (Wang et al. , 2006). Hence, with increasing pH in physiological buffers the charges and the electrostatic stabilization are neutralized, resulting in aggregation of this particular MB sample.

In order to correlate the forward scattering values with the MB size, calibration beads with known sizes (2 µm, 6 µm and 10 µm) have been characterized by flow cytometer. As shown in Figure S1, a good correlation between the FSC values of the MBs and the size of the calibration beads was observed, and indeed the measured FSC values for the MBs corresponded to sizes between 2 and 6 µm.

Overall these findings show that the flow cytometry forward scattering values can be used as a parameter to evaluate the size distribution of MBs in high throughput manner, where distributions of ~15,000 MBs can be characterized within a few seconds, giving full description and quantification of the proportion of the monodisperse versus agglomerated MB sub-populations in the sample.

The same approach was then applied to study the MBs in complex biological fluids (e.g., human plasma). Two different concentrations of human plasma were used in order to determine the behaviour of the MBs under *in vitro* (6% v/v plasma proteins, roughly

corresponding to 4 mg/ml proteins) and *in vivo* (full plasma proteins) conditions. Figure 5 shows the FSC and SSC for PVA MBs and a gate (labelled as P16) around the MB population. Human plasma (with no MBs) and MBs in PBS were also run as controls to set a threshold to exclude the protein background. By plotting the FSC and SSC versus the number of MBs, we found that the dispersion properties (size and size distribution) of the different MBs were not altered by transfer from PBS into human plasma since the populations overlapped completely. This indicates that no destabilisation of the MBs dispersions occurs as a result of dilution in biological fluids. When human plasma concentration was increased from 6% to 100%, the MBs showed identical distributions, indicating that their dispersion was not affected by the amount of human plasma and that the MBs retained good stability also in these conditions (Figure 5).

Physico-chemical characterization of PVA stabilised MBs after incubation in full human blood (with cells included) has also been performed in order to characterise the MBs after incubation in full blood with cells, and determine eventual binding-aggregation with the cells. As shown in Figure 6a-b, gates were set to allow to detect and count PVA stabilised MBs (P16), and when human blood alone was analysed by flow cytometry no objects with similar SSC and FSC were detected in the gated area of the MBs (Figure 6 c-d). However, when the MBs were exposed to human blood no MBs were detected in the same region (Figure 6e-f). Most probably, due to the similar size of MBs and red blood cells (erythrocytes), and large excess of erythrocytes compared to the number of MBs in full blood. As erythrocytes in blood are in the range 4.9-5.5 $\times 10^9$ per mL and the MBs added were 10^6 per mL, MB population corresponded only to 0.02% of the total number of objects in full blood, making the detection really challenging in flow cytometry. Thus, in order to better visualize and characterize the MBs in whole blood, after 1 h incubation, samples were centrifuged to pellet the blood cells while the supernatant, containing buoyant MBs, was run and characterized by flow cytometry. We found that the signal from the red blood cells was greatly decreased by the centrifugation step, due to free blood cell removal and only a small amount of blood debris was detected in the gate of the MBs (Figure 6 g-h). In this way, a much clearer signal could be observed from the MB population, as shown in the FSC and SSC plots (Figure 6 g-h). Furthermore we found that the distribution of the MBs in human blood overlapped with those dispersed in phosphate buffered saline (PBS) (Figure 7). This result confirmed that the particle size and distribution of the MBs were not significantly affected by the dispersion medium (PBS or human blood). The same approach can be applied to any large microparticles dispersed in any biological fluid.

3.2 Identification of proteins from coronas of microbubbles

To fully assess the biocompatibility of MBs, we have finally investigated the hard protein corona formation after incubation with 10% bovine serum and 6% human plasma (note that the total amount of proteins in these 2 samples is equal, with only the complement proteins being removed in the serum), in order to mimic typical *in vitro* conditions (i.e., exposure conditions used in cell studies). In addition, MBs were also incubated with full plasma (100%) to simulate the environment of the blood stream. As discussed above, current protocols to isolate particles with their protein coronas are not easily applied to MBs, as they rely on particle sedimentation under centrifugal force, whereas MBs are buoyant and thus do not sediment (Cedervall, Lynch, 2007, Monopoli, Walczyk, 2011). By taking advantage of MBs buoyancy, MBs were incubated with plasma and subsequently MB-hard protein corona complexes were isolated as described in Materials and Methods.

Interestingly, strong similarities were observed for all the different types of MBs in the protein coronas recovered after incubation in 6% and in full human plasma. As shown in Figure 8, a predominant protein band at 70 kDa, later identified as serum albumin, was consistently found in all cases. Other protein bands at 150, 80, 60, 50 and 25 kDa were also observed, with similar patterns across all the different MB samples assessed. No dramatic differences in protein band patterns were found in the coronas of the differently surface-functionalized MBs. A similar pattern was also obtained for several different kinds of MBs studied when coronas were formed in serum, rather than plasma, suggesting that the different surface properties of the MBs do not lead to a significant difference in the protein corona composition, likely due to the loss of surface curvature effects present for nanoscale particles.

Mass spectrometry (MS) was then used in order to identify the different classes of proteins in the MBs-protein coronas. The most abundant proteins identified by MS are given in Tables 2 and 3. The MS analysis confirmed that serum albumin was overall the most abundant protein in the MB-protein coronas after incubation with 6% plasma, 10% serum and full plasma. In fact, we observed that serum albumin accounts for between 8 - 55% of the total protein content in the MB coronas. The percentage varied depending on the nature of the biological fluid and the type of MBs (PVA, Type B, LBL02 and LBL04). For example, in 10% serum, the serum albumin in the MBs coronas made up over 50% of the total protein corona content for all four types of MBs. Alpha 2 glycoprotein, serotransferrin and Apolipoprotein A1, which are carrier proteins in the bloodstream to mediate the transport of ions, iron and lipids respectively, were also highly abundant within the MB protein coronas. These three proteins'

NSpC values varied in the range 16.9% - 18.5%, 5.7% - 7% and 3.1% - 8.2% respectively (Table 2). Alpha-1antiproteinase, a coagulation protein inhibitor, made up approximately 5% of the MB protein coronas. The rest of the most abundant proteins accounted for approximately 1% of the NSpC.

In 6% plasma, serum albumin was also the most abundant protein. The NSpC values of albumin for PVA, Type B, LBL02 and LBL04 MBs were between 31.6 and 46%. Several other carrier proteins were also significantly abundant, including serotransferrin and apolipoprotein B100. Immunoglobulin light chain kappa proteins were also detected among the corona proteins for all four MBs, with abundance between 6 and 15%. Complement C3 protein, a key protein of the complement protein cascade involved in blood coagulation, was associated with the MBs but in lower quantities.

Serum albumin, transferrin and apolipoprotein A1 are known as disopsonin proteins, which function to suppress phagocytosis (clearance by macrophages). In contrast, their counterpart, opsonin proteins, such as immunoglobulin and complement proteins which promote phagocytosis, were not particularly enriched in the MBs coronas (Ishida, Harashima, 2001, Owens and Peppas, 2006). Additionally, the ratio between disopsonin and opsonin proteins was high. This may suggest that the MBs in 6% plasma and 10% serum are not likely to trigger phagocytic pathways *via* their protein corona (for example, for *in vitro* cell studies), indicating a high biocompatibility of the MBs. Similarly, in full plasma, the MBs had a similar corona composition as in 6% plasma and 10% serum. However, the serum albumin showed the lowest abundance (8.1~17.1%) in full plasma, compared to 31.6 - 46% and 50.6 - 52.9% in 6% plasma and 10% serum respectively. This suggested that protein binding to MBs was significantly affected by the total protein concentrations, and that *in vitro* studies may not be entirely predictive of *in vivo* behaviour. Several disopsonin proteins (e.g., serum albumin, serotransferrin and lipoproteins) were among the major components of the protein corona formed on all types of MBs (PVA, Type B, LBL02, and LBL04) also in full plasma, however several opsonin biomolecules were found as corona binding proteins when exposed to full plasma. In particular Immunoglobulin G and complement C3 were detected in the corona suggesting that they might promote recognition by macrophages, resulting in the potential to induce an immune response and opsonisation (Hamad et al. , 2010). However, the presence of these biomolecules in the corona does not directly imply biocompatibility concerns as immunogenic epitopes of these proteins, such as the constant regions of the antibody, as they can be buried in the biomolecular corona and they might not be available for binding. (Kelly et al. , 2015). Overall the protein corona proteomics suggest high

biocompability of the MB in vitro and in vivo conditions however further studies will map the binding sites of the corona in order to fully evaluate their impact in biological environment.

4. Conclusions

We have developed and demonstrated the use of flow cytometry as a new technique to characterize the dispersions of polymer coated MBs in complex biological fluids such as human plasma and full blood where this method allows to overcome the experimental challenges associated with working with such buoyant materials. Flow cytometry sorting has also been used as an efficient novel tool to separate monodisperse MBs from multi-population dispersions (e.g. cellular and/or MB debris and MB agglomerate) even where the single MBs constituted the minority of the sample and it can be used as a useful post–synthesis cleaning step, increasing the quality of the contrast agent (Figure 3). By setting appropriate gate(s) for forward and side scattering, MBs can be isolated in less than 1h per mL of blood in an automatic manner. Importantly, this approach can also be applied to investigate interactions of such particles with full blood, and other biological media, and therefore predict the likely effective interactions between MBs and cells, *in situ*.

In addition, we believe that this method can be applied to recover the MBs after their *in vivo* exposure, such as in animal studies. The isolation of MBs by flow cytometry is relatively easy and fast compared to previously applied methods, such as phase contrast microscopy. While using high resolution microscopy only 10-100 MBs can be analyzed, within 20 min, whereas the flow cytometer can analyze more than 50,000 MBs per minute.

Thus here, we have this method to characterise multiple types of surface functionalized, polymer coated MBs, developed for multimodal imaging applications as *in vivo* contrast agents. Assessment of the composition of their protein coronas following incubation under *in vitro* (6% plasma or 10% serum) and *in vivo* (full human plasma) conditions have been carried out in order to study the biocompatibility of several representative MBs. This study shows that there is very little difference observed in terms of the proteins bound to the different types of MBs, suggesting that lack of surface curvature of the MBs may play a more prominent role than surface functionalization in driving protein binding to the MBs. Since MBs are generally in the size range of 2~6 μm in diameter, they may be large enough to

behave as flat surfaces for binding of proteins. This is very different from protein binding to nanoscale objects, where even small variations in surface properties play important roles in protein corona composition driven or enhanced by their high surface curvature.

Mass spectrometry results indicated the presence of several disopsonin proteins in the MB coronas, e.g. serum albumin, transferrin and apolipoprotein A1, which are known to suppress phagocytosis. A lack of opsonin proteins, such as immunoglobulin and complement proteins which are known to promote phagocytosis, was observed in 10% serum treated MBs. Additionally, it was found that since the ratio between disopsopin and opsonin proteins was fairly high, MBs existing in *in vitro* conditions may indicate higher biocompatibility of MBs that is actually the case *in vivo*.

Acknowledgments:

This work was supported by the European Union's Seventh Framework Programme (EU FP7) under grant agreement Nanosolutions (grant agreement 309329), QualityNano (grant agreement 262163), 3MICRON (grant agreement 245572) an SFI PI Award (12/IA/1422; awarded to KD) and SFI Industry fellowship (15/IFA/3057; awarded to MM).

References

Aggarwal P, Hall JB, McLeland CB, Dobrovolskaia MA, McNeil SE. Nanoparticle interaction with plasma proteins as it relates to particle biodistribution, biocompatibility and therapeutic efficacy. Adv Drug Deliv Rev. 2009;61:428-37.

Bigdeli A, Palchetti S, Pozzi D, Hormozi-Nezhad MR, Baldelli Bombelli F, Caracciolo G, et al. Exploring Cellular Interactions of Liposomes Using Protein Corona Fingerprints and Physicochemical Properties. ACS nano. 2016.

Boraschi D, Costantino L, Italiani P. Interaction of nanoparticles with immunocompetent cells: nanosafety considerations. Nanomedicine (Lond). 2012;7:121-31.

Brismar TB, Grishenkov D, Gustafsson B, Harmark J, Barrefelt A, Kothapalli SV, et al. Magnetite nanoparticles can be coupled to microbubbles to support multimodal imaging. Biomacromolecules. 2012;13:1390-9.

Camner P, Lundborg M, L. L, Gerde P, Gross N, Jarstrand C. Experimental and calculated parameters on particle phagocytosis by alveolar macrophages. Journal of Applied Physiology. 2002;92:2608-16.

Casals E, Pfaller T, Duschl A, Oostingh GJ, Puntes V. Time evolution of the nanoparticle protein corona. ACS nano. 2010;4:3623-32.

Cavalieri F, El Hamassi A, Chiessi E, Paradossi G. Stable polymeric microballoons as multifunctional device for biomedical uses: synthesis and characterization. Langmuir : the ACS journal of surfaces and colloids. 2005;21:8758-64.

Cedervall T, Lynch I, Lindman S, BerggÃ¥rd T, Thulin E, Nilsson H, et al. Understanding the nanoparticleâ€“protein corona using methods to quantify exchange rates and affinities of proteins for nanoparticles. Proceedings of the National Academy of Sciences. 2007;104:2050.

Cerroni B, Chiessi E, Margheritelli S, Oddo L, Paradossi G. Polymer shelled microparticles for a targeted doxorubicin delivery in cancer therapy. Biomacromolecules. 2011;12:593-601.

Colvin VL. The potential environmental impact of engineered nanomaterials. Nature biotechnology. 2003;21:1166-70.

de Gennes PG. Polymers at an interface; a simplified view. Advances in Colloid and Interface Science. 1987;27:189-209.

Ferrari M. Cancer nanotechnology: opportunities and challenges. Nat Rev Cancer. 2005;5:161-71.

Gao Z, Kennedy AM, Christensen DA, Rapoport NY. Drug-loaded nano/microbubbles for combining ultrasonography and targeted chemotherapy. Ultrasonics. 2008;48:260-70.

Ge C, Du J, Zhao L, Wang L, Liu Y, Li D, et al. Binding of blood proteins to carbon nanotubes reduces cytotoxicity. Proceedings of the National Academy of Sciences. 2011;108:16968-73.

Hadjidemetriou M, Al-Ahmady Z, Mazza M, Collins RF, Dawson K, Kostarelos K. In Vivo Biomolecule Corona around Blood-Circulating, Clinically Used and Antibody-Targeted Lipid Bilayer Nanoscale Vesicles. ACS nano. 2015a;9:8142-56.

Hadjidemetriou M, Al-Ahmady Z, Mazza M, Collins RF, Dawson K, Kostarelos K. In Vivo Biomolecule Corona around Blood-Circulating, Clinically Used and Antibody-Targeted Lipid Bilayer Nanoscale Vesicles. ACS nano. 2015b;9:8142-56.

Hamad I, Al-Hanbali O, Hunter AC, Rutt KJ, Andresen TL, Moghimi SM. Distinct polymer architecture mediates switching of complement activation pathways at the nanosphere-serum interface: implications for stealth nanoparticle engineering. ACS nano. 2010;4:6629-38.

He W, Yang F, Wu Y, Wen S, Chen P, Zhang Y, et al. Microbubbles with surface coated by superparamagnetic iron oxide nanoparticles. Materials Letters. 2012;68:64-7.

Ishida T, Harashima H, Kiwada H. Interactions of liposomes with cells in vitro and in vivo: opsonins and receptors. Current Drug Metabolism. 2001;2:397-409.

Kelly PM, Aberg C, Polo E, O'Connell A, Cookman J, Fallon J, et al. Mapping protein binding sites on the biomolecular corona of nanoparticles. Nature nanotechnology. 2015;10:472-9.

Konduru NV, Tyurina YY, Feng W, Basova LV, Belikova NA, Bayir H, et al. Phosphatidylserine targets single-walled carbon nanotubes to professional phagocytes in vitro and in vivo. PloS one. 2009;4:e4398.

Kumar A, Bicer EM, Morgan AB, Pfeffer PE, Monopoli M, Dawson KA, et al. Enrichment of immunoregulatory proteins in the biomolecular corona of nanoparticles within human respiratory tract lining fluid. Nanomedicine : nanotechnology, biology, and medicine. 2016.

Lesniak A, Fenaroli F, Monopoli MP, Aberg C, Dawson KA, Salvati A. Effects of the Presence or Absence of a Protein Corona on Silica Nanoparticle Uptake and Impact on Cells. ACS nano. 2012;6:5845-57.

Lunov O, Syrovets T, Loos C, Beil J, Delacher M, Tron K, et al. Differential uptake of functionalized polystyrene nanoparticles by human macrophages and a monocytic cell line. ACS nano. 2011;5:1657-69.

Mahmoudi M, Shokrgozar MA, Sardari S, Moghadam MK, Vali H, Laurent S, et al. Irreversible changes in protein conformation due to interaction with superparamagnetic iron oxide nanoparticles. Nanoscale. 2011;3:1127-38.

Maiolo D, Del Pino P, Metrangolo P, Parak WJ, Baldelli Bombelli F. Nanomedicine delivery: does protein corona route to the target or off road? Nanomedicine (Lond). 2015;10:3231-47.

Milani S, Baldelli Bombelli F, Pitek AS, Dawson KA, Radler J. Reversible Versus Irreversible Binding of Transferrin to Polystyrene Nanoparticles: Soft and Hard Corona. ACS nano. 2012;6:2532-41.

Monopoli MP, Aberg C, Salvati A, Dawson KA. Biomolecular coronas provide the biological identity of nanosized materials. Nature nanotechnology. 2012;7:779-86.

Monopoli MP, Walczyk D, Campbell A, Elia G, Lynch I, Baldelli Bombelli F, et al. Physical-Chemical Aspects of Protein Corona: Relevance to in Vitro and in Vivo Biological Impacts of Nanoparticles. Journal of the American Chemical Society. 2011.

Nel AE, Mädler L, Velegol D, Xia T, Hoek EMV, Somasundaran P, et al. Understanding biophysicochemical interactions at the nano-bio interface. Nature materials. 2009;8:543-57.

Owens DE, Peppas NA. Opsonization, biodistribution, and pharmacokinetics of polymeric nanoparticles. International journal of pharmaceutics. 2006;307:93-102.

Palchetti S, Colapicchioni V, Digiacomo L, Caracciolo G, Pozzi D, Capriotti AL, et al. The protein corona of circulating PEGylated liposomes. Biochimica et biophysica acta. 2016;1858:189-96.

Peyratout CS, Dahne L. Tailor-made polyelectrolyte microcapsules: from multilayers to smart containers. Angew Chem Int Ed Engl. 2004;43:3762-83.

Raesch SS, Tenzer S, Storck W, Rurainski A, Selzer D, Ruge CA, et al. Proteomic and Lipidomic Analysis of Nanoparticle Corona upon Contact with Lung Surfactant Reveals Differences in Protein, but Not Lipid Composition. ACS nano. 2015;9:11872-85.

Rocker C, Potzl M, Zhang F, Parak WJ, Nienhaus GU. A quantitative fluorescence study of protein monolayer formation on colloidal nanoparticles. Nature nanotechnology. 2009;4:577-80.

Sund J, Alenius H, Vippola M, Savolainen K, Puustinen A. Proteomic characterization of engineered nanomaterial-protein interactions in relation to surface reactivity. ACS nano. 2011;5:4300-9.

Tenzer S, Docter D, Kuharev J, Musyanovych A, Fetz V, Hecht R, et al. Rapid formation of plasma protein corona critically affects nanoparticle pathophysiology. Nature nanotechnology. 2013;8:772-81.

Walczyk D, Bombelli FB, Monopoli MP, Lynch I, Dawson KA. What the cell "sees" in bionanoscience. Journal of the American Chemical Society. 2010;132:5761-8.

Walkey CD, Chan WCW. Understanding and controlling the interaction of nanomaterials with proteins in a physiological environment. Chemical Society Reviews. 2012;41:2780-99.

Wan S, Kelly PM, Mahon E, Stockmann H, Rudd PM, Caruso F, et al. The "sweet" side of the protein corona: effects of glycosylation on nanoparticle-cell interactions. ACS nano. 2015;9:2157-66.

Wang QZ, Chen XG, Liu N, Wang SX, Liu CS, Meng XH, et al. Protonation constants of chitosan with different molecular weight and degree of deacetylation. Carbohydrate Polymers. 2006;65:194-201.

Yan Y, Gause KT, Kamphuis MM, Ang CS, O'Brien-Simpson NM, Lenzo JC, et al. Differential roles of the protein corona in the cellular uptake of nanoporous polymer particles by monocyte and macrophage cell lines. ACS nano. 2013;7:10960-70.

Zybailov B, Mosley AL, Sardiu ME, Coleman MK, Florens L, Washburn MP. Statistical analysis of membrane proteome expression changes in Saccharomyces cerevisiae. J Proteome Res. 2006;5:2339-47.

Figure Captions

Figure 1. Flow cytometry and microscopy analysis of Type B MBs dispersed in PBS. (a) Forward scattering distribution (FSC-A); (b) double scatter plot of side scattering versus forward scatering of Type B MBs obtained by flow cytometry. Different gates are applied (as indicated by the different colors) in order to distinguish MBs with low FSC (blue) from those with medium (green, sorted medium) and high (purple, sorted high) FSC. These gates have been applied to sort the different MB sub-populations; (c) Phase contrast image of unsorted Type B MBs; (d-e) Phase contrast micrographs of the seperated fractions of Type B MBs with high FSC (sorted high) and medium FSC (sorted medium), respectively, from (b). (f) Enlargement of MBs from (e).

Figure 2. Flow cytometry and microscopy analysis of LBL03 MBs dispersed in PBS. (a) Forward scattering distribution (FSC-A); (b) double scatter plot of side scattering versus forward scatering of LBL03 MBs obtained by flow cytometry. Different gates are applied (as indicated by the different colors) in order to distinguish MBs with low FSC (blue) from those with medium (green, sorted medium) and high (purple, sorted high) FSC. These gates have been applied to sort the different MB sub-populations; (c) Phase contrast image of unsorted LBL03 MBs; (d-e) Phase contrast micrographs of the seperated fractions of LBL03 MBs with high FSC (sorted high) and medium FSC (sorted medium), respectively, from (b). (f) Enlargement of MBs from (e).

Figure 3. Flow cytometry and microscopy analysis of LBL08 MBs dispersed in PBS. (a) Forward scattering distribution (FSC-A); (b) double scatter plot of side scattering versus forward scatering of LBL08 MBs obtained by flow cytometry. Different gates are applied (as indicated by the different colors) in order to distinguish MBs with low FSC (blue) from those with medium (green, sorted medium) and high (purple) FSC. These gates have been applied to sort the different MB sub-populations; (c) Phase contrast image of unsorted LBL08 MBs; (d-e) Phase contrast micrographs of the separated fractions of LBL08 MBs with high FSC (sorted high) and medium FSC (sorted medium), respectively, from (b). (f) Enlargement of MBs from (e).

Figure 4. Flow cytometry and microscopy analysis of PVA MBs dispersed in PBS. (a) Forward scattering distribution (FSC-A); (b) double scatter plot of side scattering versus forward scatering of PVA MBs obtained by flow cytometry. Different gates are applied (as indicated by the different colors) in order to distinguish MBs with low FSC (blue) from those

with medium (green, sorted medium) and high (purple, sorted high) FSC. These gates have been applide to sort the different MB sub-populations; (c) Phase contrast image of unsorted PVA MBs; (d-e) Phase contrast micrographs of the separated fractions of PVA MBs with high FSC (sorted high) and medium FSC (sorted medium), respectively, from (b). (f) Enlargement of MBs from (e).

Figure 5. (a) Flow cytometry scatter plot of FSC and SSC of (from the left) full plasma, PVA-MBs dispersed in PBS, PVA-MBs in 6% plasma and PVA-MBs in full plasma. A gate, set as P16, was made to mark the MB population only omitting the background. (b-c) Flow cytometry plots of FSC and SSC relative to the number of events counted in P16 for PVA-MBs in plasma under (b) *in vitro* conditions and (c) *in vivo* conditions (red line).

Figure 6. PVA MB characterization by flow cytometry in full blood. (a) FSC and SSC of PVA MBs dispersed in PBS (b) Magnification of gated area that contains MBs. (c) FSC and SSC of full blood; (d) Magnification of gated area that contains MBs. (e) FSC and SSC of PVA MBs in full blood; (f) Magnification of gated area containing MBs. (g) FSC and SSC of MBs in full blood following centrifugation to reduce the background scattering from erythrocytes, resulting in more accurate visualization of the PVA MBs by flow cytometry . (b), (d), (f) and (h) are the enlargement of the MBs populations (red outlines) in the graphs (a), (c), (e) and (g) respectively.

Figure 7. FSC (a) and SSC (b) distribution by flow cytometry of PVA MBs in PBS (black line) and in full blood (red line).

Figure 8. SDS-PAGE gel showing a comparison of the protein coronas associated with the different types of MBs after incubation with 6% plasma (a), 10% serum (b), and full plasma (c).

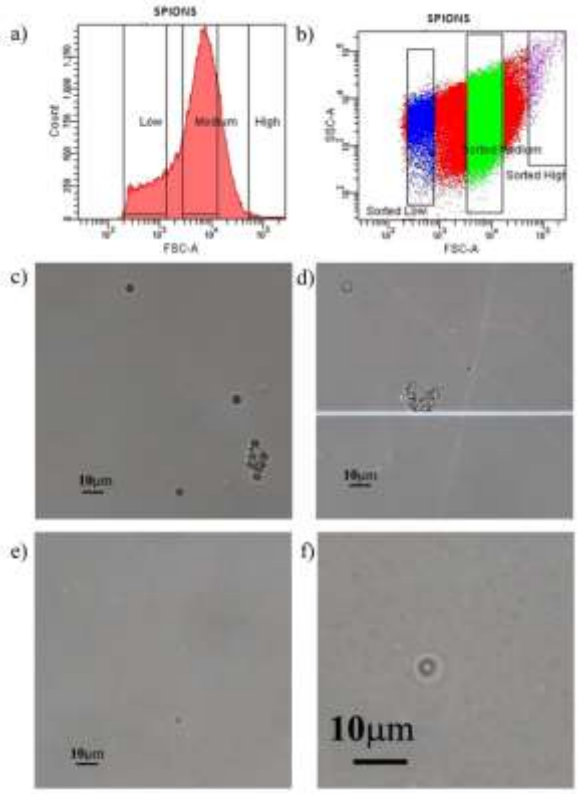

Figure 1

Figure 2

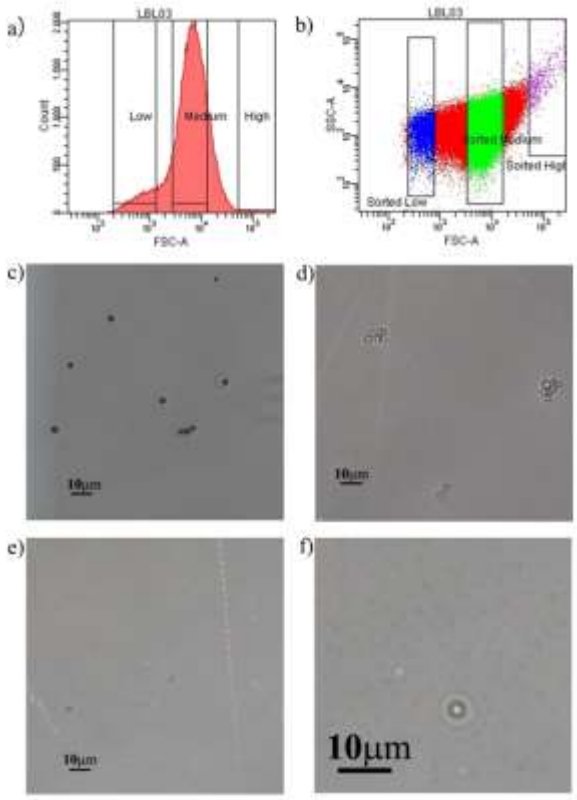

Figure 3

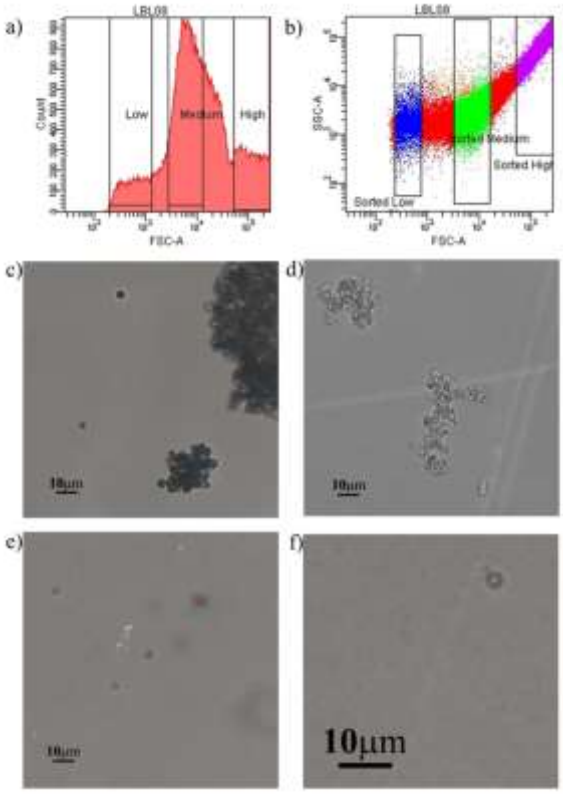

Figure 4

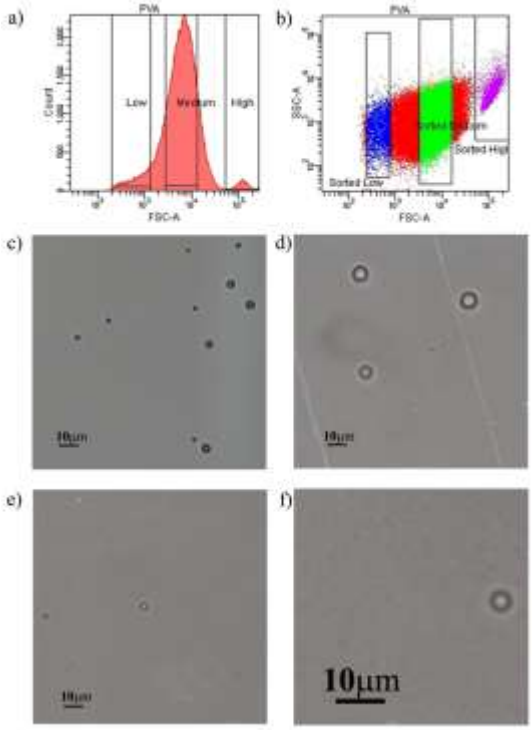

Figure 5

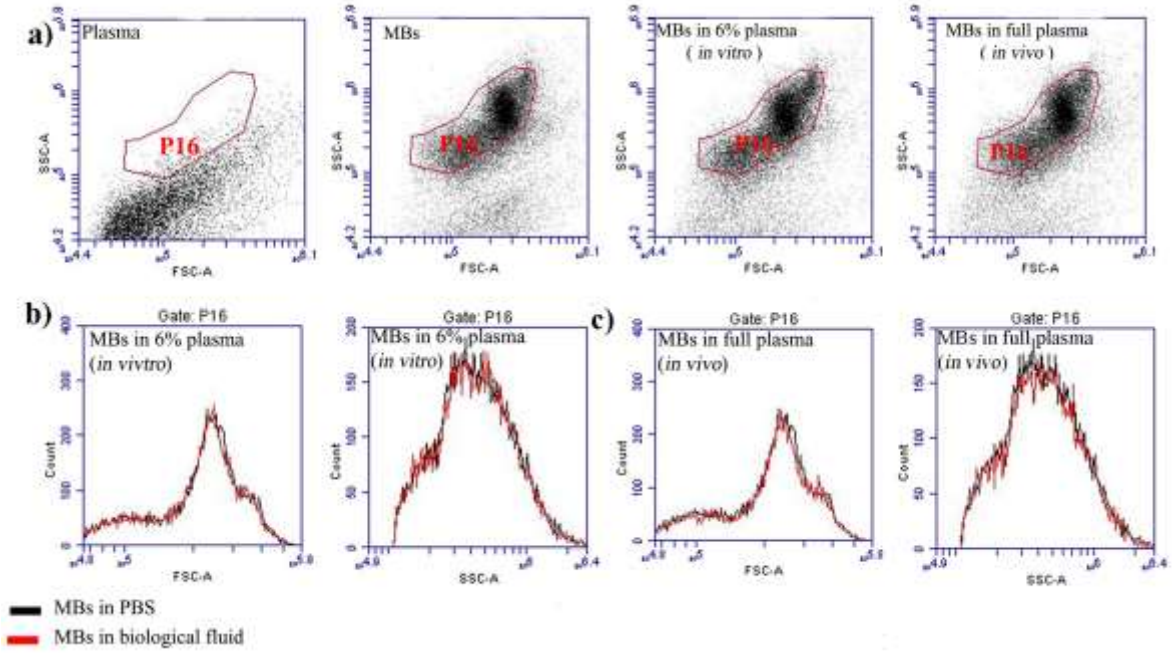

Figure 6

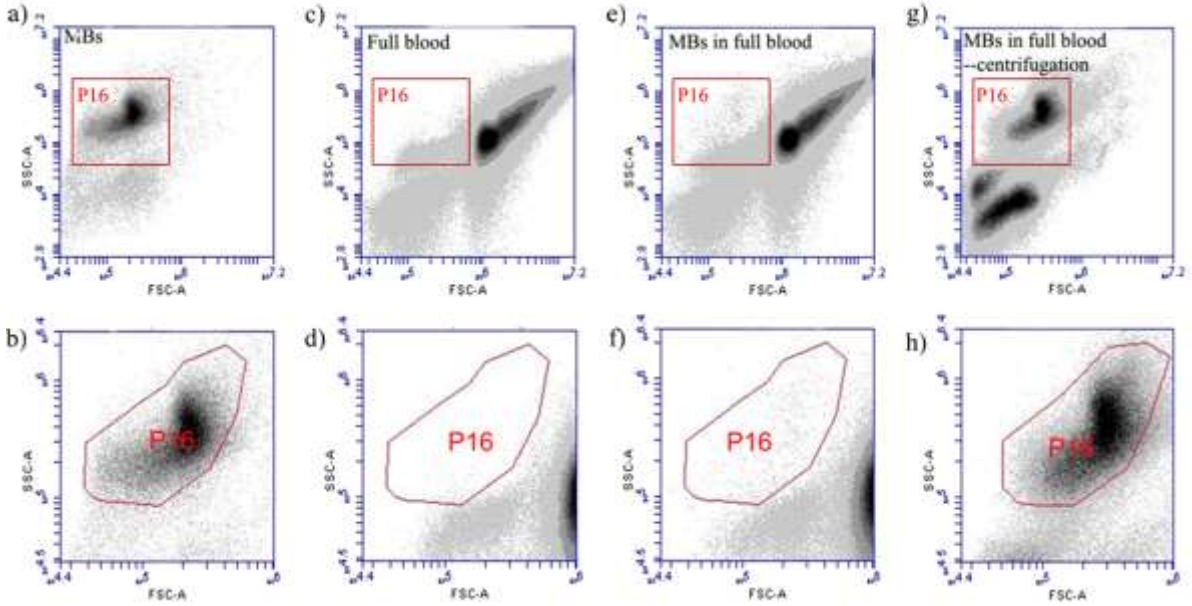

Figure 7

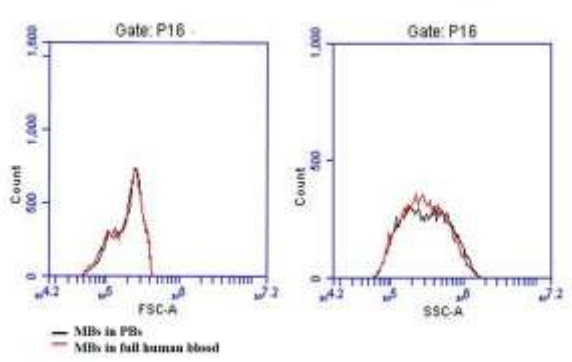

Figure 8

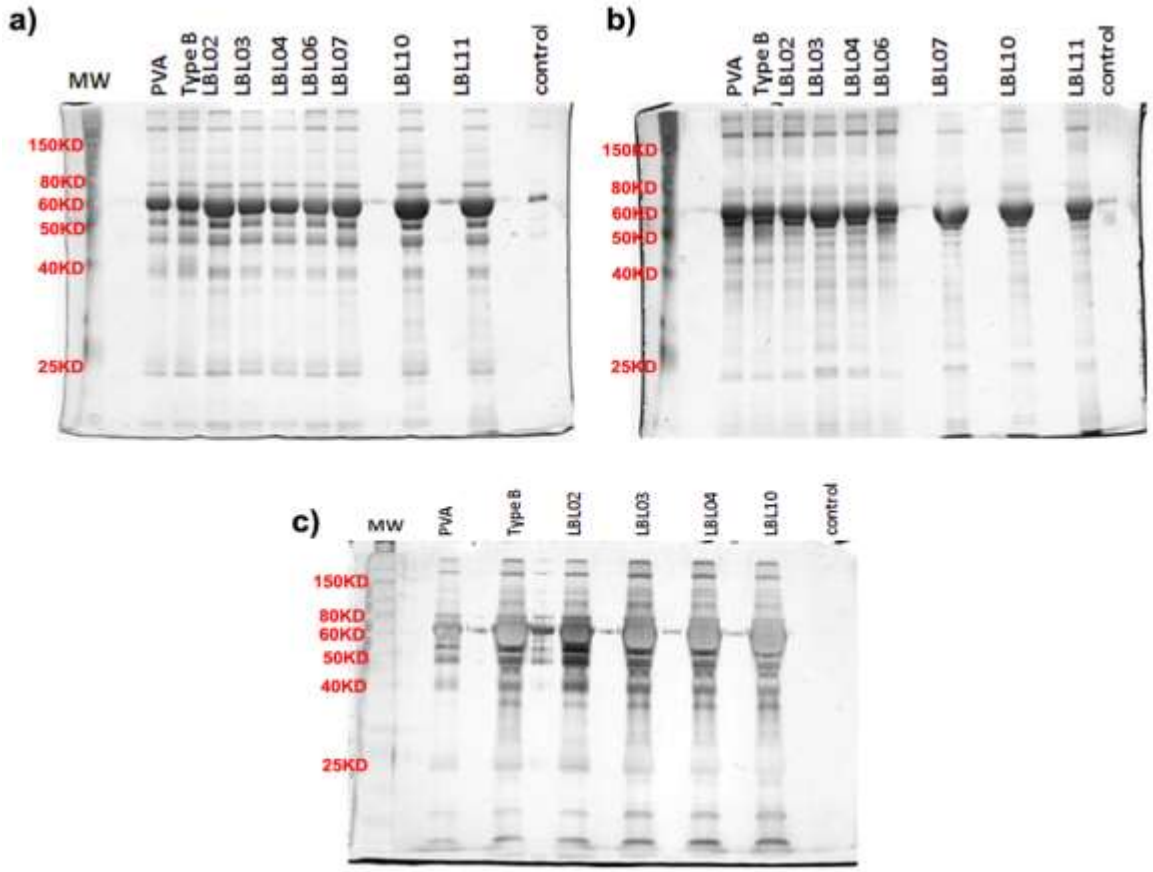

Table 1. Summary descriptions of the MBs used in the study in terms of their composition and outer surface layer charge.

Name	**Inner layer**	**outer layer**	**Charge of the outmost layer**
PVA	-	-	-
TypeB	-	-	-
LBL02	AG	-	positive
LBL03	AG	PSS	negative
LBL04	AG	PMAA	negative
LBL06	AG	Albumin	negative
LBL07	AG/PSS	PAH	positive
LBL08	AG/PSS	Chitosan	positive
LBL10	AG/PSS	PAOEt	positive
LBL11	AG/PSS	PDA	positive

PVA: poly(vinyl alcohol); Type B: superparamagnetic iron oxide nanoparticles embedded in PVA shell; AG: aminoguanidine; PSS: Polystyrene sulfonate; PMAA: (Poly(methacrylic acid), PAH: (polyallyalmine), PAOEt: (Poly(methacryloxyethyltrimethylammonium) bromide, PDA: (Poly(diallyldimethylammonium chloride)

Table 2. MS analysis of protein coronas associated with MBs (PVA, Type B, LBL02 and LBL04) under *in vitro* conditions (MBs incubated in 10% serum or 6% plasma). Protein abundance is expressed as the Spectral Count (Spc) and Normalised SpC (NSPc).

10% Serum (*in vitro* conditions)			**SpC**				**NSpC**			
Accession	**Protein indentity**	**Mw (Da)**	**PVA**	**TypeB**	**LBL02**	**LBL04**	**PVA**	**TypeB**	**LBL02**	**LBL04**
P02769	Serum albumin	69249	155	190	188	209	52.9	52.4	50.6	52.9
P12763	Alpha 2 glycoprotein	38394	30	34	37	39	18.5	16.9	18.0	17.8
Q29443	Serotransferrin	77703	22	23	33	31	6.7	5.7	7.9	7.0
P34955	Alpha-1antiproteinase	46075	10	11	13	12	5.1	4.6	5.3	4.6
Q7SIH1	Alpha-2macroglobulin	167470	8	16	19	16	1.1	1.8	2.1	1.7
P15497	Apolipoprotein A-I	30258	4	13	11	11	3.1	8.2	6.8	6.4

6% plasma (*in vitro* conditions)			**SpC**				**NSpC**			
Accession	**Protein indentity**	**Mw (Da)**	**PVA**	**TypeB**	**LBL02**	**LBL04**	**PVA**	**TypeB**	**LBL02**	**LBL04**
P02768	Serum albumin	69322	414	319	430	279	31.6	45.8	40.8	46.6
P01857	Ig gamma 1 chain	36083	58	26	43	24	8.5	7.2	7.8	7.7
P01023	Alpha 2macroglobulin	163187	51	13	36	5	1.7	0.8	1.5	0.4
P02787	Serotransferrin	77014	42	27	52	23	2.9	3.5	4.4	3.5
P01024	Complement C3	187029	41	53	40	38	1.2	2.8	1.4	2.4
P04114	Apolipoprotein B100	515284	39	76	52	64	0.4	1.5	0.7	1.4
P01834	Ig kappa chain C region	11602	34	8	19	9	15.5	6.9	10.8	9.0
P00738	Haptoglobin	45177	21	8	23	0	2.5	1.8	3.3	0.0

Table 3. MS analysis of protein coronas associated with MBs (PVA, Type B, LBL02 and LBL04) under *in vivo* conditions (MBs incubated in full plasma). Protein abundance is expressed as the Spectral Count (Spc) and Normalised SpC (NSPc).

Full plasma (*in vivo* conditions) **SpC**

Accession	Protein Identity	Mw (Da)	PVA	Type B	LBL02	LBL04
P02768	Serum albumin	69322	154	152	170	296
P01834	Ig kappa chain C region	11602	15	8	26	56
P02787	Serotransferrin	77014	67	45	60	138
P01620	Ig kappa chain V-III	11768	7	3	4	13
P01857	Ig gamma-1 chain	36083	17	10	15	40
P01009	Alpha-1-antitrypsin	46707	21	11	20	53
P02647	Apolipoprotein A-I	30759	13	2	22	36
P02675	Fibrinogen beta chain	55892	22	8	17	43
B9A064	Ig lambda-1	23049	8	12	10	23
P01024	Complement C3	187029	60	57	88	154

Full plasma *(in vivo* conditions*)*

NSpC

Accession	Protein Identity	Mw (Da)	PVA	Type B	LBL02	LBL 04
P02768	Serum albumin	69322	11.4	17.1	8.1	8.4
P01834	Ig kappa chain C	11602	6.6	5.4	7.4	9.5
P02787	Serotransferrin	77014	4.5	4.6	2.6	3.5
P01620	Ig kappa chain V-III	11768	3.1	2.0	1.1	2.2
P01857	Ig gamma-1 chain	36083	2.4	2.2	1.4	2.2
P01009	Alpha-1-antitrypsin	46707	2.3	1.8	1.4	2.2
P02647	Apolipoprotein A-I	30759	2.2	0.5	2.4	2.3
P02675	Fibrinogen beta chain	55892	2.0	1.1	1.0	1.5
B9A064	Ig lambda-1	23049	1.8	4.1	1.4	2.0
P01024	Complement C3	187029	1.6	2.4	1.6	1.6